Tailoring the Energy Landscape of Graphene Nanostructures on Graphene and Manipulating Them Using Tilt Grain Boundaries

Yi-Wen Liu,[†] Chen-Yue Hao,[†] and Lin He [*]

Center for Advanced Quantum Studies, Department of Physics, Beijing Normal University, Beijing, 100875, People's Republic of China

In two-dimensional van der Waals (vdW) materials, the relative twist angle between adjacent layers not only controls their electronic properties but also determines their stacking energy. This effect makes it difficult to stabilize the vdW materials with twist angles. Here, we demonstrate that we can controllably stabilize the system with custom-designed twist angles, for example, magic angle, which is realized by tailoring the adhesive-energy landscape of graphene nanostructures on graphene by using a one-dimensional tilt grain boundary (GB). Our result demonstrates that the flat band of the custom-built nanoscale magic-angle-twisted bilayer graphene is still robust, even when its size is comparable to a single moiré spot. Moreover, in our experiments, the area ratio with different stacking orders separated by the tilt GB can be continuously tuned by using the scanning-tunneling-microscope tip, and we can repeatedly fold and unfold the graphene nanostructure along the one-dimensional GB, demonstrating the ability to manipulate the graphene nanostructure at the atomic scale.

I. INTRODUCTION

In van der Waals (vdW) layered materials, the physical properties crucially depend on the relative twist angle between adjacent layers [1–5]. The most reputed example is bilayer graphene, in which we can obtain two-dimensional quasicrystals [6–8], magic-angle-twisted bilayer graphene with flat bands [9–11], minimally twisted bilayer graphene with a triangular network of chiral one-dimensional states [12–15], and so on, by simply varying the relative twist angle. The structures and corresponding stacking energy in bilayer graphene also depend on the relative twist angle. Bilayer graphene with stacking misorientation is energetically unstable and the zero-twist-angle stacking order, i.e., the Bernal-stacked bilayer, is the most energetically favorable structure [16–19]. Consequently, thermal fluctuations can lead to rotation between the adjacent vdW layers to the energetically favorable structure [20–26]. Therefore, stabilizing twisted bilayer graphene and achieving precise angle control are of equal importance in the development of twistronics.

Here, we demonstrate the ability to stabilize the stacking misorientation of graphene nanostructures on graphene by using a one-dimensional tilt grain boundary (GB), which is a line defect connecting two graphene grains with a relative rotated angle ϕ [27–31], in the supporting graphene. In our experiment, the area ratio with different stacking orders,

as separated by the tilt GB, of the system is continuously tuned by using a scanning-tunneling-microscope (STM) tip, which helps us to stabilize the graphene nanostructure with a tunable twist angle on graphene. Our result demonstrates that the flat band of the custom-built nanoscale magic-angle-twisted bilayer graphene is still robust even when its size is comparable to a single moiré spot. Because of the different stacking orders separated by the tilt GB, we further demonstrate that we can repeatedly fold and unfold the graphene nanostructure along the one-dimensional tilt GB.

II. EXPERIMENTAL RESULTS AND DISCUSSION

A. Calculated adhesive-energy landscape of a graphene nanostructure on graphene

For a graphene nanostructure on a continuous graphene sheet, the relative twist angle between adjacent layers plays a vital role in determining the resulting structure, as shown in Fig. 1(a). Figure 1(b) shows the calculated adhesive energy of a graphene nanostructure with 3800 carbon atoms on a continuous graphene sheet, according to the theoretical result in Ref. [18] (see Appendix A). The graphene nanostructure on graphene is initially of AB (or Bernal) stacking, defined as zero-twist angle, and the adhesive energy depends sensitively on the relative twist angle. The energy maxima for twist angles of 20° and 40° are set to zero [18]. Obviously, the AB-stacked configuration is the most stable stacking order, and the 30° configuration is a metastable stacking order. The configurations with

―――――――
[*]helin@bnu.edu.cn
[†]Y.-W. Liu and C.-Y. Hao contributed equally to this work.

other relative twist angles are not thermally stable configurations for the graphene nanostructure on graphene. Due to the structural symmetry of graphene, the adhesive energy as a function of twist angle exhibits a period of 60°. By introducing a one-dimensional tilt GB in the supporting graphene sheet, as schematically shown in Fig. 1(a), we can controllably tune the area ratio, R_L, of the graphene nanostructure between the left side and the right side separated by the GB. This introduces a new degree of freedom, i.e., R_L, to modulate the adhesive-energy landscape of the graphene nanostructure on graphene. Figure 1(c) shows the calculated energy landscape of the graphene nanostructure on supporting graphene with a $\phi = 21°$ tilt GB (for simplicity, the boundary is assumed to be a perfect line defect with zero width, which separates the graphene structure into two parts, in the calculation). Now, the total energy of systems depends on both the twist angle and area ratio R_L separated by the GB. For the cases with $R_L = 100\%$ and 0%, there is no GB in the supporting graphene. According to Fig. 1(c), there are always one stable state and one metastable state; however, the corresponding angles of the stable state and the metastable state are not fixed but depend on the area ratio, R_L. Figure 1(d) shows representative results with area ratio $R_L = 25\%$, 50%, and 75%, which exhibit quite distinct features compared with that for $R_L = 100\%$ (or 0%).

For the $\phi = 21°$ tilt GB, the stable state and the metastable state can be switched by changing the area ratio, R_L. Moreover, the twist angle of two regions separated by the GB can be continuously tuned from 9° to 0° (pink circles in Fig. 1) and from 21° to 30° (black circles in Fig. 1), respectively, by changing the area ratio from 0% to 100% (see Fig. 5 in Appendix A for the energy landscape of another tilt GB).

B. Stabilizing the graphene nanostructure by the tilt grain boundary

To explore the above effects experimentally, highly oriented pyrolytic graphite (HOPG) and multilayer graphene on Ni foil synthesized by chemical vapor deposition (see Appendix B) are used in our experiments. Previous studies have demonstrated that one-dimensional tilt GBs with different ϕ can be frequently observed in the two systems [27–31], which is also observed in our STM measurement (see Fig. S1 within the Supplemental Material [32] for STM characterizations of grain boundaries). The graphene nanostructures are obtained by etching the studied samples with the hydrogen-plasma etching method (see Figs. S2 and S3 within the Supplemental Material
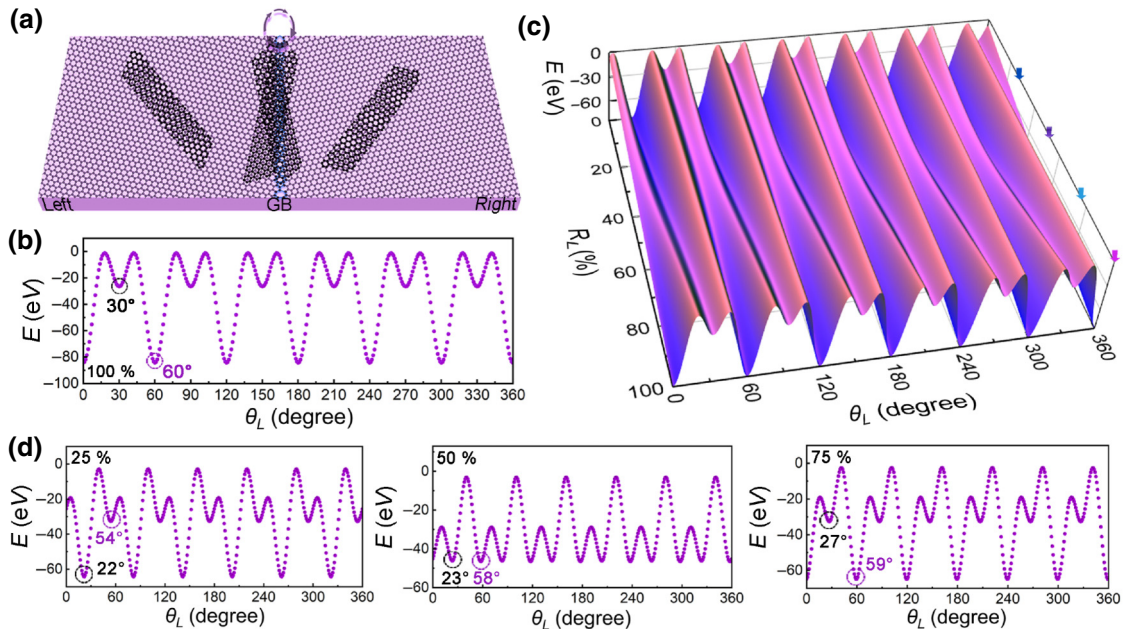

FIG. 1. Energy landscape of graphene nanostructure on graphene with a tilt GB. (a) Schematic configurations of a graphene nanostructure on graphene with a tilt GB. (b) Energy evolution of a graphene nanostructure on single-crystal graphene with different relative twist angles. (c) Energy landscape of a graphene nanostructure on graphene with a tilt GB. In this theoretical energy landscape, the tilt angle of the GB is 21°, as observed in our experiment (Figs. 2–4), and the area of the nanostructure is 100 nm². Parameter θ_L represents the twist angle of the graphene nanostructure with underlying graphene on the left of the GB. R_L is defined as the area ratio between the region on the left of the GB and the whole nanostructure. (d) Energy evolution as a function of twist angle. Area ratios are about 25%, 50%, and 75%. Area ratio and twist angle of the stable or metastable state are strongly related. By changing the area ratio, the twist angle for the metastable and stable states can be changed gradually.

[32] for STM characterizations of graphene nanostructures). To study the effects of the tilt GB on the stacking orders of the graphene nanostructures on graphene, we use a STM tip to "move" an etched graphene nanostructure

to a selected tilt GB. Figures 2(a)–2(d) summarize two typical processes in our experiments. Reducing the tunneling resistance and moving the tip along a given direction, the graphene nanostructure can be repeatedly
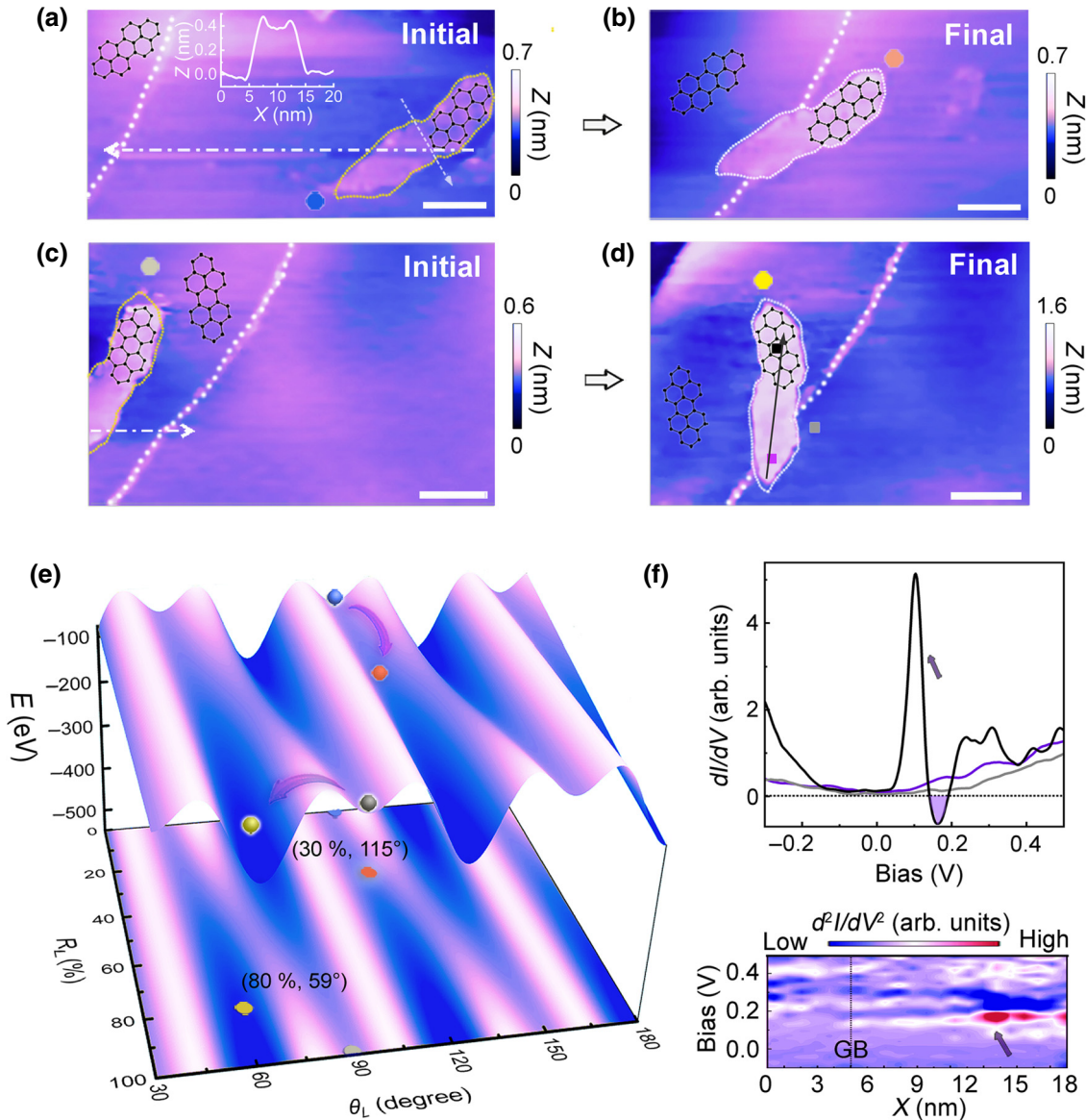

FIG. 2. Stabilizing the graphene nanostructure by the tilt GB. (a) STM image of an initial configuration showing that the graphene nanostructure is on the right side of the GB. GB is highlighted with the white dotted line. Inset, height profile of the graphene nanostructure along the white arrow. (b) STM image of a final configuration that the graphene nanostructure is "moved" on top of the GB, $V_s = 1$ V and $I = 0.1$ nA. Area ratio is measured to be about 30%, and the twist angle is measured to be about $115° \pm 1.0°$. Obtained nanostructure is moved along the white arrow by the tip with $V_s = 1$ V and $I = 0.2$ nA in (a). (c) STM image of an initial configuration showing that the nanostructure is in the left side of the GB ($V_s = 1$ V and $I = 0.1$ nA). (d) STM image of a final configuration that the nanostructure is "moved" on top of the GB with an area ratio of about 80% and twist angle of about $60° \pm 1.0°$. Scale bar, 10 nm ($V_s = 1$ V and $I = 0.1$ nA). Nanostructure is moved along the white arrow in panel (c) by the STM tip with $V_s = 1$ V and $I = 0.8$ nA. (e) Corresponding states in the energy landscape of the configurations in (a)–(d). Blue and gray dots indicate the initial states in (a) and (c). Yellow and orange dots show the final states in (b) and (d). Area ratio and twist angle of these states are marked with (R_L, θ_L). Twist angles are measured by comparing atomic resolved images of top and bottom graphene sheets. (f) Top, STS map is recorded along the black arrow in (d). Bottom, STS spectra are obtained at three typical positions marked by the colored square dots in (d). Flat band is marked by arrows.

moved on and off the tilt GB (see Fig. S4 within the Supplemental Material [32] for the movement of graphene nanostructures). Our experiments indicate that the graphene nanostructure on the tilt GB is quite stable during measurements and the graphene nanostructure becomes movable only when the STM tip approaches to manipulate it (the STM tip approaches the graphene nanostructure by either decreasing the bias or increasing the current or both of them, see Fig. S5 within the Supplemental Material [32] as an example). To fully understand the experimental results, we carry out atomic resolved STM measurements (see Figs. S6 and S7 within the Supplemental Material [32] for the atomic resolved images). The rotated angle of crystal orientation between the left and right sides of the tilt GB in the supporting graphene is about $21.1° \pm 1.0°$, and the relative twist angles, θ_L, of the graphene nanostructure to the left region of the tilt GB in Figs. 2(a)–2(d) are also measured. According to the area ratio, R_L, and twist angle, θ_L, with the left side of the GB, we can obtain the detected initial and final states in Figs. 2(a)–2(d) on the energy landscape, as summarized in Fig. 2(e) (see Appendix A for detailed calculations). There is mainly a translation of the graphene nanostructure from panel (a) to panel (b), whereas there are translation and rotation of the graphene nanostructure from panel (c) to panel (d). Because of the large rotation angle, the manipulation from panel (c) to panel (d) overcomes a barrier of the energy landscape.

The final configurations in Figs. 2(b) and 2(d) are in the valleys of the energy landscape, indicating that they are energetically favorable states, as observed in our experiment. The competition from adhesive energy between the two regions separated by the tilt GB helps to stabilize the configurations with stacking misorientations in the studied system. For the final configuration in Fig. 2(d), the twist angle between the graphene nanostructure and the left side of the GB is about 1° (near the magic angle). To study the local electronic structure, we carry out scanning-tunneling-spectroscope (STS) measurements (see Appendix C for STM and STS measurements), as summarized in Fig. 2(f). A pronounced tunneling peak is clearly observed on the graphene nanostructure on the left side of the GB [Fig. 2(f), top panel]. Such a feature is attributed to the flat bands in magic-angle-twisted bilayer graphene (MATBG). In addition, there is negative differential conductance between the flat bands and the steplike features in the spectrum, which is a clear signature of a gap between the flat band and the high-energy bands in slightly TBG, as observed previously [12,33–35]. Therefore, our result demonstrates that the flat band of MATBG is still robust when its size is comparable to a single moiré spot. Due to the different stacking orders separated by the tilt GB, the two regions exhibit quite different electronic properties, and a clear boundary is observed, as shown in the bottom panel of Fig. 2(f).

C. Tunable configurations of the nanostructure on graphene with the tilt grain boundary

Recent experiments demonstrated the ability to tune strained structures of graphene by using local probing tips [36–45]. In our experiments, the continuously tunable area ratio enables us to realize almost countless stable and metastable states for the graphene nanostructure on graphene. By using the STM tip, the transfer between stable and metastable states, i.e., from either stable states to metastable states or from metastable states to stable states, can be realized. Figures 3(a)–3(c) summarize three representative results obtained in our experiments and each figure shows composite STM images to compare the states before and after each manipulation step. The initial and final configurations of the graphene nanostructure on the tilt GB are seized in the STM measurements and the corresponding states on the energy landscape are obtained, as shown in Fig. 3(d), according to the area ratio and twist angle with the left side of the GB (see Fig. S8 within the Supplemental Material [32] for the enlarged atomic resolved images and the moiré pattern image). From the energy landscape, the relationship between twist angle, area ratio, and total energy can be vividly displayed. When the area ratio is close to 50%, the two regions separated by the tilt GB are stabilized in configurations with stacking misorientation. Increasing the difference in the area between two regions, e.g., $R_L = 20\%$ or 80%, the region with a large area becomes nearly aligned with the supporting graphene. Obviously, the changes in the configurations of the graphene nanostructure correspond to the switch between the stable states and the metastable states.

D. Custom-designed manipulation of the graphene nanostructure using the tilt grain boundary

Due to the existence of the tilt GB, the two regions of the graphene nanostructure, as separated by the tilt GB, exhibit different stacking orders. Therefore, the vdW forces between the two regions of the graphene nanostructure and the underlying graphene are different. Such a feature provides us with an unprecedented opportunity to fold the graphene nanostructure at a selected position, as schematically shown in Fig. 4(a). By decreasing the distance between the STM tip and the graphene nanostructure, we can lift and fold the graphene nanostructure at the position of the tilt GB when the tip-graphene vdW force overcomes the force between the graphene nanostructure and the underlying graphene. Figure 4(b) shows a typical experimental result. The scanning bias is decreased from 1 V to 50 mV stepwise with an interval of 50 mV (the tunneling current is fixed at 0.1 nA). Then, the left side of the graphene nanostructure can be lifted and folded at the position along the tilt GB under a scanning bias
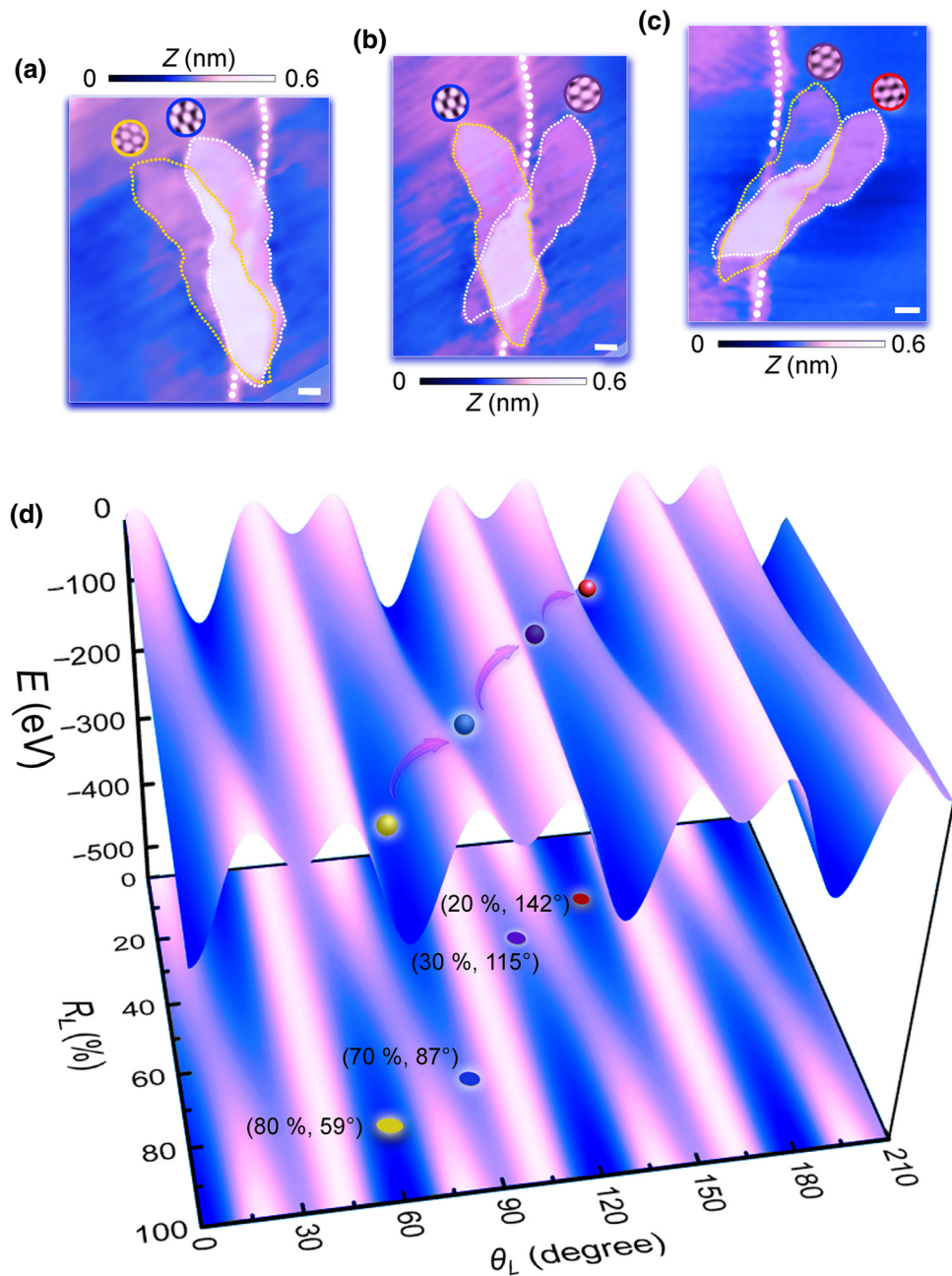
FIG. 3. Tunable configurations of the nanostructure on graphene with the tilt GB. (a) Configurations before (yellow) and after (blue) the first tip manipulation. STM images taken at 1 V and 0.1 nA. Nanostructure is rotated by the tip with $V_s = 1$ V and $I = 0.8$ nA. (b) STM images before (blue) and after (purple) the second operation. Nanostructure is rotated by the tip with $V_s = 1$ V and $I = 0.8$ nA. (c) STM image before (purple) and after (red) the third manipulation. Nanostructure is rotated by the tip with $V_s = 150$ mV and $I = 0.1$ nA. Scale bar, 4 nm. Atomic resolved images are marked with colored circles in (a)–(c). (d) Corresponding states in the energy landscape of the configurations in (a)–(c). Corresponding states are identified with colored dots with the area ratio and the twist angle (R_L, θ_L).

of 50 mV (see Fig. S9 within the Supplemental Material [32] for the folding and unfolding processes, see Appendix D for the estimation of the tip-graphene distance and vdW forces). The continuously tunable area ratio of the graphene nanostructure enables us to fold and unfold

the graphene nanostructure at any selected position, as demonstrated in Figs. 4(b)–4(d). Although folding and unfolding graphene nanostructures along an arbitrarily chosen direction were realized very recently [33], folding and unfolding the graphene nanostructures at the nanoscale
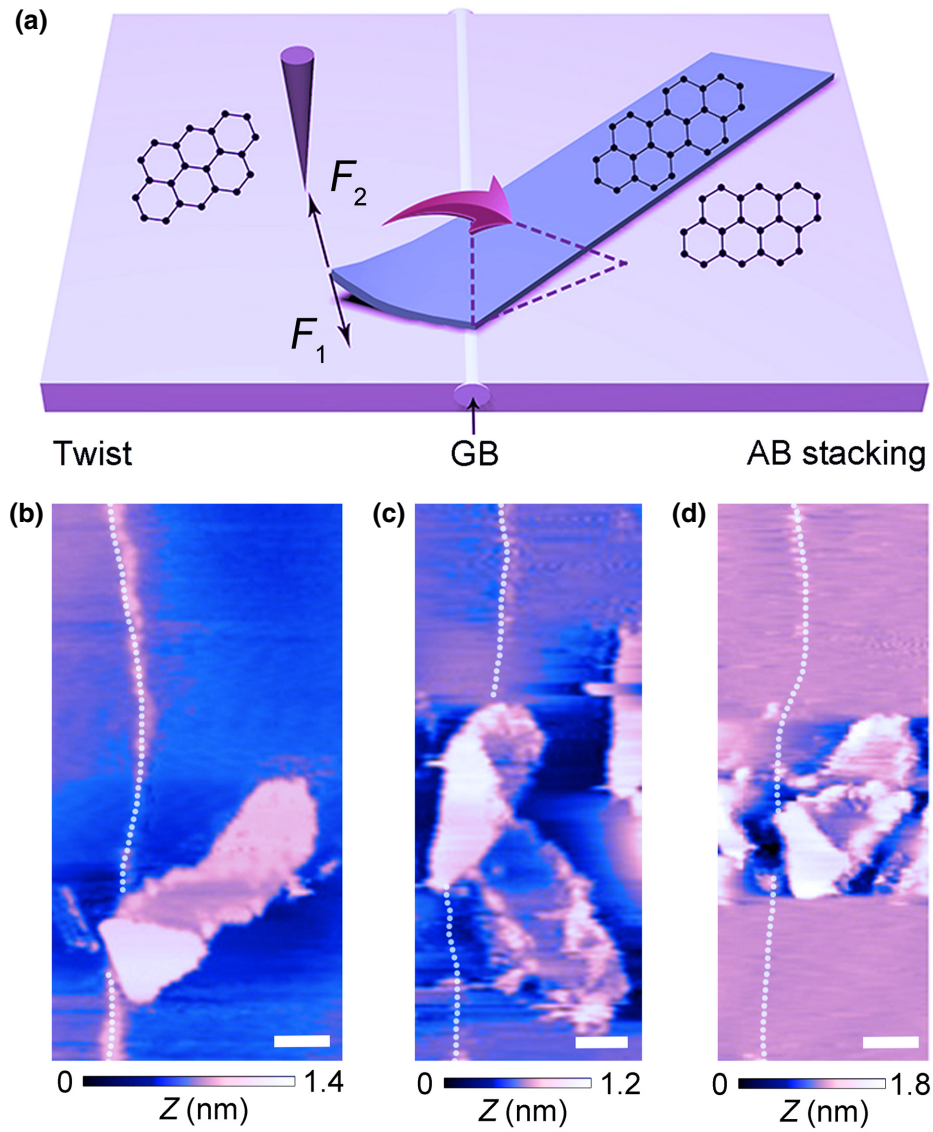
FIG. 4. Custom-designed manipulation of the graphene nanostructure using the GB. (a) Schematic showing the process of folding the graphene nanostructure along the tilt GB by using a tip. F_1 is the vdW force between the graphene nanostructure and the underlying graphene. F_2 is the vdW force between the tip and the graphene nanostructure. Purple dotted line is the final configuration after folding. (b)–(d) STM images of the nanostructure after folding. Nanostructure is the same as that in Figs. 2 and 3. Tunneling current used for folding is $I = 0.1$ nA. Left side of the nanostructure with weaker interlayer interactions is folded to the right side along the GB. Scale bar, 10 nm. More and more "contaminants," which may be gas molecules or nanoflakes of etched graphene adsorbed on the tip, adsorb on the graphene nanostructure during the folding process because of the large tip-sample vdW force.

at custom-designed positions are still very big challenges in experiments. Our results provide a promising route to overcome this challenge with the help of the one-dimensional tilt GB.

III. CONCLUSION

Using a one-dimensional tilt GB in the supporting graphene, we provide a method to tailor the adhesive energy of graphene nanostructures on graphene. The tunable area ratio with different stacking orders, as

separated by the tilt GB, of the system helps us to stabilize the graphene nanostructure with tunable twist angles on graphene, which is of vital importance in the development of twistronics. It is interesting to find that the flat band of the custom-built nanoscale magic-angle-twisted bilayer graphene is still robust, even when its size is comparable to a single moiré spot. Because the different stacking orders are separated by the tilt GB, the graphene nanostructure can be folded and unfolded along the GB, which shows the ability to manipulate the graphene nanostructure at the atomic scale. The *in situ* manipulation and

measurements reported in our experiments are the beginning of the study of the twist-dependent electronic properties of van der Waals materials at the nanoscale, which may lead to the possible development of twist-based nanodevices.

APPENDIX A: DETAILS OF THE ENERGY CALCULATION

1. Total energy of the nanosystem

In our experiment, the total number of atoms of the graphene nanostructure is about 8000, which is much larger than the number of carbon atoms, about 4000, of the large graphene flake in Ref. [18]. Therefore, we use the results obtained for the large graphene flake in Ref. [18] to calculate the energy landscape. We calculate the total energy from

$$E_{LR} = A_{LR} N E_{lr}. \qquad (A1)$$

Here, E_{LR} represents the total energy of the flake for the left or the right area of the GB, A_{LR} is the area to the left or right side of the GB, N is the number of atoms per unit area, and E_{lr} is the energy per atom at a certain twist angle for the left or right side of the GB. The total energy can be obtained by summing the energy of the right side and the

left side of the boundary. For the bilayer system, the number of atoms is doubled. Since the increased area and layers influence only the total energy, rather than changing the main characteristics of the three-dimensional energy-state diagram, we simplify the total energy with the nanoflake of the top layer. The number of atoms per unit area is approximately 38 nm^{-2}.

2. The influences on the energy calculation

Here, we discuss some factors that may influence the total energy of the landscape.

(1) Edge atoms: According to previous theoretical work [18], there are fewer edge effects for a large flake compared with a small flake. In our experiments, the number of edge atoms of the graphene nanostructure is about 500, which is about 6% of the total number of atoms, and the energy of the edge atoms is assumed to be the same as that inside the nanostructure in our calculations.

(2) Interlayer distance: The interlayer distance between the nanostructure and the supporting graphene layer is assumed as 0.32 nm (here, we should point out that using an interlayer distance of 0.36 nm does not affect the main features of the energy landscape nor the main results of this work).

(3) Stacking order: In our experiments, the stacking orders of the graphene nanostructure on graphene are directly measured by using atomic resolved STM images. Then, we can calculate the stacking energy of the graphene nanostructure on graphene.

(4) Lateral motion: The route from one stacking configuration to the other configuration cannot be exactly
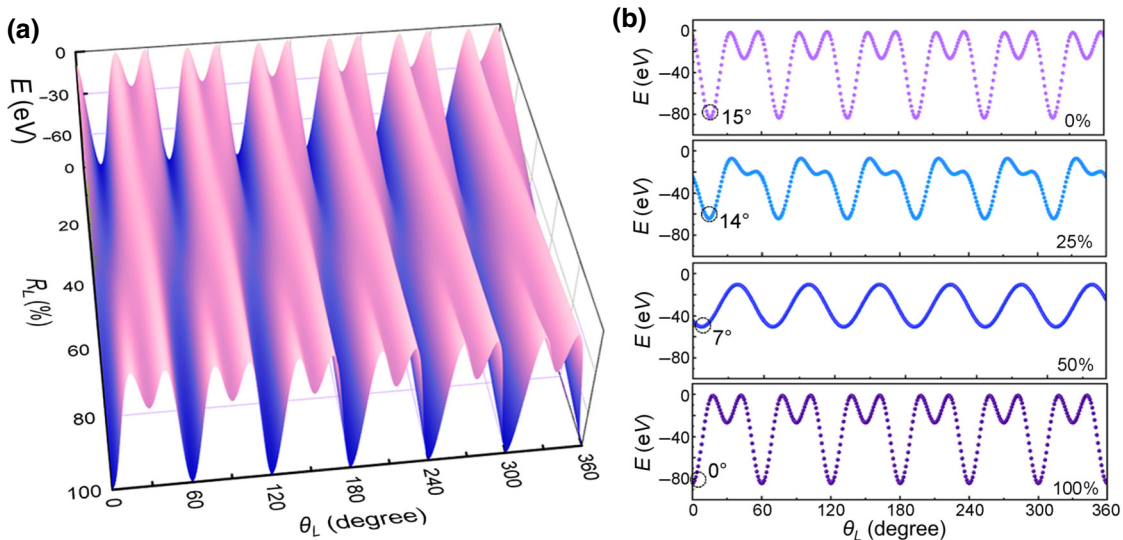

FIG. 5. (a) Energy landscape of graphene nanostructure on graphene with a $\phi = 15°$ tilt GB. Area of the nanostructure is 100 nm^2. (b) Energy evolution as a function of twist angle for area ratios of 0%, 25%, 50%, and 100%. Angles of stable states marked with black circles are about 15°, 14°, 7°, and 0°. Changing the area ratio from 0% to 100%, the stacking misorientation with the left side of the GB can be tuned from 15° to 0°.
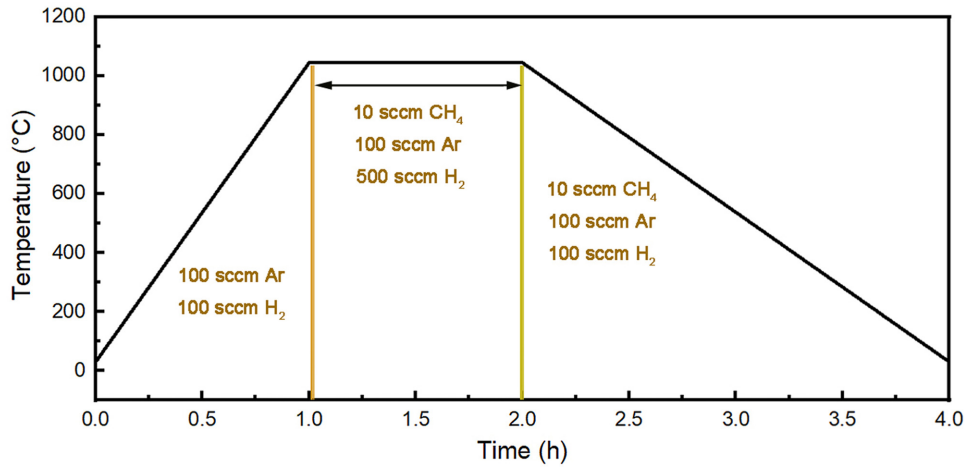
FIG. 6.   Temperature program for growth by the LPCVD method. After growth, multilayer graphene with one-dimensional boundaries can be obtained. Then, we repeat this procedure and change the middle step into 100 sccm Ar, 100 sccm H_2, 70 W power to obtain nanoflakes.

detected by using STM and is not the topic of this work. Therefore, it is not necessary to take into account the effects of lateral motion and rotation on our result. Only the stacking orders of the initial configuration and the final configuration are important in this work.

(5) Temperature: In Ref. [18], the energy landscape of graphene nanostructures on graphene is calculated at 0 K. Our experiments are carried out at 77 K, and the studied stacking configurations of the graphene nanostructure on graphene are quite stable at 77 K. The switching between different stacking configurations of the graphene nanostructure on graphene is achieved only with the help of the STM tip, and thermal fluctuation does not activate the switching between different states. Therefore, it is reasonable to assume that temperature does not affect the main feature of the energy landscape of graphene nanostructures on graphene.

(6) Boundary effect: Here, the effect of the width of the tilt grain boundary (about 0.5 nm) is not taken into account, and the boundary is assumed to be a perfect line defect with zero width in the calculations. First, we consider that the GB is equally divided into two parts so that it can affect the nanostructure on both sides of the GB equally. Here, we calculate the effective atomic percentage of the GB for the nanostructure. For the final states in Figs. 2(b) and 2(d) of the main text, the length of the GB, the number of atoms, and the atomic percentage are about 13 nm, 247 atoms, and 3% and 11 nm, 209 atoms, and 2.6%, respectively. In addition, for the states in Figs. 3(a)–3(c), the length of the GB, the number of atoms, and the atomic percentage are about 11 nm, 209 atoms, 2.6%; 18 nm, 342 atoms, 4.2%; 17 nm, 323 atoms, 4% and 9 nm, 171 atoms, 2%. All of the proportions are less than 5%. From the estimation of the number of atoms above, we find that they are not dominant
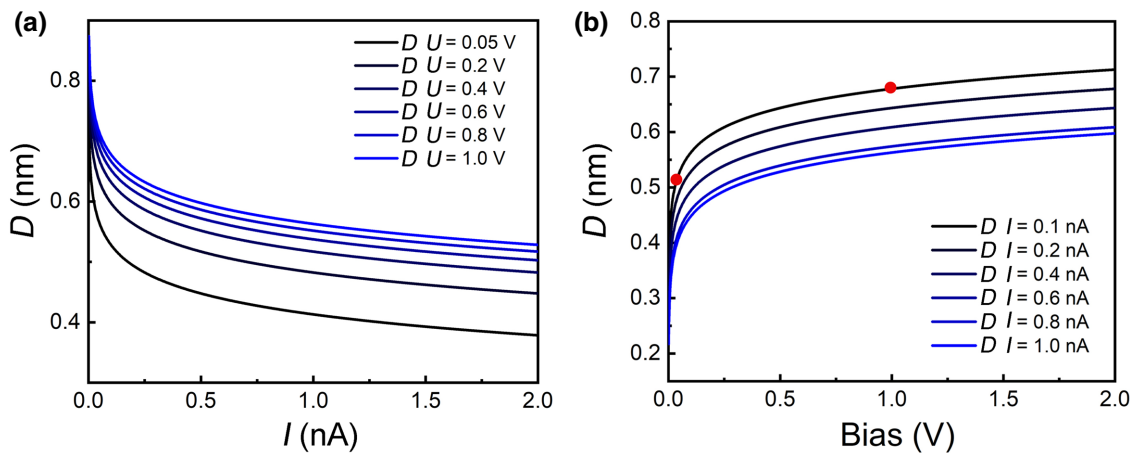

FIG. 7.   (a) Tip-sample distance decreases with increasing current. (b) Tip-sample distance increases with increasing bias. Red dots represent the tip height at 1 V and 0.05 V with a fixed tunneling current of 0.1 nA.
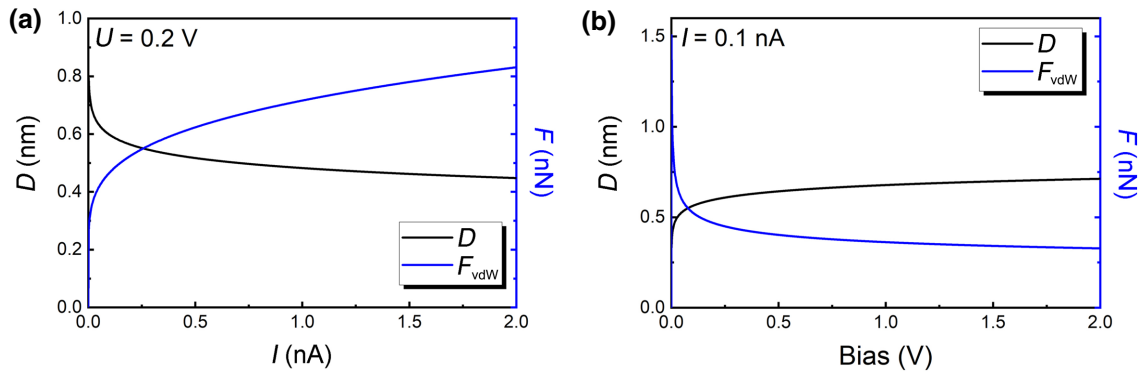
FIG. 8. (a) Tip-sample distance and tip-sample van der Waals forces as the function of current at a fixed sample bias of 0.2 V. (b) Tip-sample distance and van der Waals forces as the function of bias at a fixed current of 0.1 nA.

factors in the whole system. Second, the final states in the energy landscape are always located at energy valleys at a fixed area ratio. This tells us that the competing adhesive energy is the dominant reason in our experiments, and the movements can be described very well without including the GB/edge effects. The theoretical energy landscape is consistent with the movements of the nanostructure, which can support our simplified estimations.

(7) Substrate influence: Theoretically, the energy landscape is determined by the atomic stacking configurations of the two adjacent pristine graphene layers. When the substrate introduces large lattice reconstruction and local strain from the graphene layers, then the energy landscape is expected to be strongly affected. In our experiments, the topmost graphene layer is atomically flat, and there is no detectable lattice reconstruction and local strain. Therefore, it is reasonable to use the theoretical calculation to understand our experimental results for the graphene nanostructure on graphene.

(8) Isolated bilayer vs graphene on multilayers: The van der Waals forces decay quickly with increasing interlayer distance [46]. The distance between the third layer and the top layer is larger than 0.6 nm, which indicates that the van der Waals potential energy between them is close to zero in our experiments. Different from the energy states, there are some problems related to size effects and boundary effects for the local density of states. These questions are worthy of further study. Here, we focus on the construction and manipulation of the TBG system.

APPENDIX B: SAMPLE PREPARATION

Multilayer graphene on Ni foil is synthesized by using low-pressure chemical vapor deposition (LPCVD). First, the substrate is put on a quartz shelf in a 2-inch quartz tube, and then it is annealed at a temperature of about 1045 °C for 1 h with 100 sccm (standard cubic centimeters per minute) Ar and 100 sccm H_2. Next, 10 sccm CH_4 and 500 sccm H_2 are added to synthesize graphene

for about 60 min. Finally, the sample is cooled to room temperature under 100 sccm Ar and 100 sccm H_2 naturally. In this work, we use multilayer graphene on Ni foil and HOPG substrate to obtain one-dimensional tilt boundaries [31]. The graphene nanostructures are obtained by putting multilayer graphene in hydrogen-plasma LPCVD [47] (Fig. 6).

APPENDIX C: STM AND STS MEASUREMENTS

STM measurements are taken in an ultrahigh vacuum chamber with a pressure of about 10^{-11} Torr with (USM-1400 and USM-1500) STM systems (UNISOKU). All measurements are carried out in constant-current scanning mode. Lateral dimensions of the STM topographic measurements are calibrated using a standard graphene lattice, a Si (111) 7×7 lattice, and Ag (111) surface. The STM tips are obtained by chemical etching from a wire of Pt-Ir (80/20%) alloy. The experiments are performed at a temperature of about 77 K. The STS spectra are recorded with a standard lock-in technique by turning off the feedback circuit and using a 793-Hz 5-mV ac modulation of the sample voltage.

APPENDIX D: TIP-SAMPLE DISTANCE AND VAN DER WAALS FORCES

To further understand our experimental results, we can simply estimate the tip-sample distance and van der Waals forces between the tip and the nanostructure. The tip-sample distance can be estimated according to [38,40,41, 44,48–50]

$$D(I, V) = \frac{1}{2c} \ln \left(\frac{V}{IR_0} \right). \tag{D1}$$

Here, V and I are the bias and current in the experiments, and R_0 and c depend on the tip-sample contact; R_0 is $\hbar/2e^2$ and $c \sim 1$ Å^{-1}. The calculated results are shown in Fig. 7. The van der Waals forces between the tip and the

nanostructure can be estimated according to [23,51]

$$F_{\mathrm{vdW}} = \frac{AR}{6D^2}. \tag{D2}$$

Here, R is the radius of the tip, A is the Hamaker constant of 1×10^{-19} J, and D is the tip-sample distance. The order of the forces is about 0.1–1 nN. With increasing current or decreasing bias, the tip height becomes smaller and the van der Waals forces between tip and nanostructure increase, as shown in Fig. 8. When the van der Waals force between the tip and graphene nanostructure is larger than the force between the graphene nanostructure and substrate, the nanostructure is lifted up.

For the folding process in our experiments, we decrease the bias from 1 V to 50 mV at a fixed current of 0.1 nA. Based on the above analysis, the tip height changes from 0.68 to 0.53 nm, accordingly. Correspondingly, the van der Waals force between the tip and flake changes from 0.36 to 0.6 N. The flake is lifted up at 50 mV, which means that F_{vdW} between the tip and flake is larger than the F_{vdW} between the flake and substrate at a height of 0.53 nm.

[1] A. K. Geim and I. V. Grigorieva, Van der Waals heterostructures, Nature **499,** 419 (2013).

[2] K. Novoselov, A. Mishchenko, A. Carvalho, and A. C. Neto, 2D materials and van der Waals heterostructures, Science **353,** aac9439 (2016).

[3] L. Balents, C. R. Dean, D. K. Efetov, and A. F. Young, Superconductivity and strong correlations in moiré flat bands, Nat. Phys. **16,** 725 (2020).

[4] E. Y. Andrei and A. H. MacDonald, Graphene bilayers with a twist, Nat. Mater. **19,** 1265 (2020).

[5] Y.-N. Ren, Y. Zhang, Y.-W. Liu, and L. He, Twistronics in graphene-based van der Waals structures, Chin. Phys. B **29,** 117303 (2020).

[6] S. J. Ahn, P. Moon, T.-H. Kim, H.-W. Kim, H.-C. Shin, E. H. Kim, H. W. Cha, S.-J. Kahng, P. Kim, M. Koshino, Y.-W. Son, C.-W. Yang, and J. R. Ahn, Dirac electrons in a dodecagonal graphene quasicrystal, Science **361,** 782 (2018).

[7] W. Yao, E. Wang, C. Bao, Y. Zhang, K. Zhang, K. Bao, C. K. Chan, C. Chen, J. Avila, M. C. Asensio, J. Zhu, and S. Zhou, Quasicrystalline 30° twisted bilayer graphene as an incommensurate superlattice with strong interlayer coupling, Proc. Natl. Acad. Sci. U. S. A. **115,** 6928 (2018).

[8] C. Yan, D.-L. Ma, J.-B. Qiao, H.-Y. Zhong, L. Yang, S.-Y. Li, Z.-Q. Fu, Y. Zhang, and L. He, Scanning tunneling microscopy study of the quasicrystalline 30° twisted bilayer graphene, 2D Mater. **6,** 045041 (2019).

[9] L.-J. Yin, J.-B. Qiao, W.-J. Zuo, W.-T. Li, and L. He, Experimental evidence for non-abelian gauge potentials in twisted graphene bilayers, Phys. Rev. B **92,** 081406 (2015).

[10] Y. Cao, V. Fatemi, A. Demir, S. Fang, S. L. Tomarken, J. Y. Luo, J. D. Sanchez Yamagishi, K. Watanabe, T. Taniguchi, E. Kaxiras, R. C. Ashoori, and P. Jarillo-Herrero, Unconventional superconductivity in magic-angle graphene superlattices, Nature (London) **556,** 80 (2018).

[11] Y. Cao, V. Fatemi, S. Fang, K. Watanabe, T. Taniguchi, E. Kaxiras, and P. Jarillo-Herrero, Unconventional superconductivity in graphene superlattices, Nature (London) **556,** 43 (2018).

[12] Y.-W. Liu, Y. Su, X.-F. Zhou, L.-J. Yin, C. Yan, S.-Y. Li, W. Yan, S. Han, Z.-Q. Fu, Y. Zhang, Q. Yang, Y.-N. Ren, and L. He, Tunable Lattice Reconstruction, Triangular Network of Chiral one-Dimensional States, and Bandwidth of Flat Bands in Magic Angle Twisted Bilayer Graphene, Phys. Rev. Lett. **125,** 236102 (2020).

[13] S. Huang, K. Kim, D. K. Efimkin, T. Lovorn, T. Taniguchi, K. Watanabe, A. H. MacDonald, E. Tutuc, and B. J. LeRoy, Topologically Protected Helical States in Minimally Twisted Bilayer Graphene, Phys. Rev. Lett. **121,** 037702 (2018).

[14] J.-B. Qiao, L.-J. Yin, and L. He, Twisted graphene bilayer around the first magic angle engineered by heterostrain, Phys. Rev. B **98,** 235402 (2018).

[15] S. G. Xu, A. I. Berdyugin, P. Kumaravadivel, F. Guinea, R. K. Kumar, D. A. Bandurin, S. V. Morozov, W. Kuang, B. Tsim, S. Liu, J. H. Edgar, I. V. Grigorieva, V. I. Fal'ko, M. Kim, and A. K. Geim, Giant oscillations in a triangular network of one-dimensional states in marginally twisted graphene, Nat. Commun. **10,** 4008 (2019).

[16] M. Reguzzoni, A. Fasolino, E. Molinari, and M. C. Righi, Potential energy surface for graphene on graphene: Ab initio derivation, analytical description, and microscopic interpretation, Phys. Rev. B **86,** 245434 (2012).

[17] S. Zhou, J. Han, S. Dai, J. Sun, and D. J. Srolovitz, Van der Waals bilayer energetics: Generalized stacking-fault energy of graphene, boron nitride, and graphene/boron nitride bilayers, Phys. Rev. B **92,** 155438 (2015).

[18] F. Peymanirad, S. K. Singh, H. Ghorbanfekr-Kalashami, K. Novoselov, F. Peeters, and M. Neek-Amal, Thermal activated rotation of graphene flake on graphene, 2D Mater. **4,** 025015 (2017).

[19] S. Bagchi, H. Johnson, and H. Chew, Rotational stability of twisted bilayer graphene, Phys. Rev. B. **101,** 054109 (2020).

[20] D. Wang, *et al.*, Thermally Induced Graphene Rotation on Hexagonal Boron Nitride, Phys. Rev. Lett. **116,** 126101 (2016).

[21] Q. Zheng, B. Jiang, S. Liu, Y. Weng, L. Lu, Q. Xue, J. Zhu, Q. Jiang, S. Wang, and L. Peng, Self-retracting Motion of Graphite Microflakes, Phys. Rev. Lett. **100,** 067205 (2008).

[22] Z. Liu, J. Yang, F. Grey, J. Z. Liu, Y. Liu, Y. Wang, Y. Yang, Y. Cheng, and Q. Zheng, Observation of Microscale Superlubricity in Graphite, Phys. Rev. Lett. **108,** 205503 (2012).

[23] X. Feng, S. Kwon, J. Y. Park, and M. Salmeron, Superlubric sliding of graphene nanoflakes on graphene, ACS Nano **7,** 1718 (2013).

[24] M. Dienwiebel, G. S. Verhoeven, N. Pradeep, J. W. Frenken, J. A. Heimberg, and H. W. Zandbergen, Superlubricity of Graphite, Phys. Rev. Lett. **92,** 126101 (2004).

[25] C. Qu, S. Shi, M. Ma, and Q. Zheng, Rotational Instability in Superlubric Joints, Phys. Rev. Lett. **122,** 246101 (2019).

[26] K. Wang, C. Qu, J. Wang, B. Quan, and Q. Zheng, Characterization of a Microscale Superlubric Graphite Interface, Phys. Rev. Lett. **125**, 026101 (2020).

[27] J. Lahiri, Y. Lin, P. Bozkurt, I. I. Oleynik, and M. Batzill, An extended defect in graphene as a metallic wire, Nat. Nanotechnol. **5**, 326 (2010).

[28] Z. Fei, A. S. Rodin, W. Gannett, S. Dai, W. Regan, M. Wagner, M. K. Liu, A. S. McLeod, G. Dominguez, M. Thiemens, Antonio H. Castro Neto, F. Keilmann, A. Zettl, R. Hillenbrand, M. M. Fogler, and D. N. Basov, Electronic and plasmonic phenomena at graphene grain boundaries, Nat. Nanotechnol. **8**, 821 (2013).

[29] R. Grantab, V. B. Shenoy, and R. S. Ruoff, Anomalous strength characteristics of tilt grain boundaries in graphene, Science **330**, 946 (2010).

[30] P. Y. Huang, C. S. Ruiz-Vargas, A. M. van der Zande, W. S. Whitney, M. P. Levendorf, J. W. Kevek, S. Garg, J. S. Alden, C. J. Hustedt, Y. Zhu, J. Park, P. L. McEuen, and D. A. Muller, Grains and grain boundaries in single-layer graphene atomic patchwork quilts, Nature (London) **469**, 389 (2011).

[31] L.-J. Yin, J. B. Qiao, W. X. Wang, Z.-D. Chu, K. F. Zhang, R.-F. Dou, C.-L. Gao, J.-F. Jia, J.-C. Nie, and L. He, Tuning structures and electronic spectra of graphene layers with tilt grain boundaries, Phys. Rev. B **89**, 205410 (2014).

[32] See the Supplemental Material at http://link.aps.org/supplemental/10.1103/PhysRevApplied.17.034013 for more experimental data and details of the analysis.

[33] Y.-N. Ren, C. Lu, Y. Zhang, S. Y. Li, Y.-W. Liu, C. Yan, Z.-H. Guo, C.-C. Liu, F. Yang, and L. He, Spectroscopic evidence for a spin-and valley-polarized metallic state in a nonmagic-angle twisted bilayer graphene, ACS Nano **14**, 13081 (2020).

[34] S. Y. Li, Y. Zhang, Y.-N. Ren, S. J. Liu, X. Dai, and L. He, Experimental evidence for orbital magnetic moments generated by moiré-scale current loops in twisted bilayer graphene, Phys. Rev. B **102**, 121406 (2020) (Rapid Communications).

[35] Y. Zhang, Z. Hou, Y.-X. Zhao, Z.-H. Guo, Y.-W. Liu, S.-Y. Li, Y.-N. Ren, Q.-F. Sun, and L. He, Correlation-induced valley splitting and orbital magnetism in a strain-induced zero-energy flatband in twisted bilayer graphene near the magic angle, Phys. Rev. B **102**, 081403 (2020) (Rapid Communications).

[36] H. Chen, X.-L. Zhang, Y.-Y. Zhang, D. Wang, D.-L. Bao, Y. Que, W. Xiao, S. Du, M. Ouyang, S. T. Pantelides, and H.-J. Gao, Atomically precise, custom-design origami graphene nanostructures, Science **365**, 1036 (2019).

[37] H. Chen, D.-L. Bao, D. Wang, Y. Que, W. Xiao, Y.-Y. Zhang, J. Sun, S. Du, and H.-J. Gao, Fabrication and manipulation of nanosized graphene homojunction with atomically-controlled boundaries, Nano Res. **13**, 3286 (2020).

[38] T. Mashoff, M. Pratzer, V. Geringer, T. Echtermeyer, M. C. Lemme, M. Liebmann, and M. Morgenstern, Bistability and oscillatory motion of natural nanomembranes appearing within monolayer graphene on silicon dioxide, Nano Lett. **10**, 461 (2010).

[39] H. S. Wong, C. Durkan, and N. Chandrasekhar, Tailoring the local interaction between graphene layers in graphite at the atomic scale and above using scanning tunneling microscopy, ACS Nano **3**, 3455 (2009).

[40] P. Xu, Y. Yang, D. Qi, S. Barber, J. Schoelz, M. Ackerman, L. Bellaiche, and P. Thibado, Electronic transition from graphite to graphene via controlled movement of the top layer with scanning tunneling microscopy, Phys. Rev. B. **86**, 085428 (2012).

[41] M. Yankowitz, K. Watanabe, T. Taniguchi, P. San-Jose, and B. J. LeRoy, Pressure-induced commensurate stacking of graphene on boron nitride, Nat. Commun. **7**, 13168 (2016).

[42] S.-Y. Li, K.-K. Bai, W.-J. Zuo, Y.-W. Liu, Z.-Q. Fu, W.-X. Wang, Y. Zhang, L.-J. Yin, J.-B. Qiao, and L. He, Tunneling spectra of a quasifreestanding graphene monolayer, Phys. Rev. Applied **9**, 054031 (2018).

[43] P. Jia, W. Chen, J. Qiao, M. Zhang, X. Zheng, Z. Xue, R. Liang, C. Tian, L. He, Z. Di, and X. Wang, Programmable graphene nanobubbles with three-fold symmetric pseudomagnetic fields, Nat. Commun. **10**, 3127 (2019).

[44] N. N. Klimov, S. Jung, S. Zhu, T. Li, C. A. Wright, S. D. Solares, D. B. Newell, N. B. Zhitenev, and J. A. Stroscio, Electromechanical properties of graphene drumheads, Science **336**, 1557 (2012).

[45] S.-Y. Li, Y. Su, Y.-N. Ren, and L. He, Valley Polarization and Inversion in Strained Graphene via Pseudo-Landau Levels, Valley Splitting of Real Landau Levels, and Confined States, Phys. Rev. Lett. **124**, 106802 (2020).

[46] J. H. Lee, A. Avsar, J. Jung, J. Y. Tan, K. Watanabe, T. Taniguchi, S. Natarajan, G. Eda, S. Adam, and A. H. Castro Neto, Van der Waals force: A dominant factor for reactivity of graphene, Nano Lett. **15**, 319 (2015).

[47] R. Yang, L. Zhang, Y. Wang, Z. Shi, D. Shi, H. Gao, E. Wang, and G. Zhang, An anisotropic etching effect in the graphene basal plane, Adv. Mater. **22**, 4014 (2010).

[48] A. Georgi, P. Nemes-Incze, R. Carrillo-Bastos, D. Faria, S. V. Kusminskiy, D. Zhai, M. Schneider, D. Subramaniam, T. Mashoff, N. M. Freitag, M. Liebmann, M. Pratzer, L. Wirtz, C. R. Woods, R. V. Gorbachev, Y. Cao, K. S. Novoselov, N. Sandler, and M. Morgenstern, Tuning the pseudospin polarization of graphene by a pseudomagnetic field, Nano Lett. **17**, 2240 (2017).

[49] D. Wong, J. Velasco, L. Ju, J. Lee, S. Kahn, H. Z. Tsai, C. Germany, T. Taniguchi, K. Watanabe, A. Zettl, F. Wang, and M. F. Crommie, Characterization and manipulation of individual defects in insulating hexagonal boron nitride using scanning tunnelling microscopy, Nat. Nanotechnol. **10**, 949 (2015).

[50] P. Xu, M. Neek-Amal, S. D. Barber, J. K. Schoelz, M. L. Ackerman, P. M. Thibado, A. Sadeghi, and F. M. Peeters, Unusual ultra-low-frequency fluctuations in freestanding graphene, Nat. Commun. **5**, 3720 (2014).

[51] L. J. Yin, W. X. Wang, K. K. Feng, J.-C. Nie, C. M. Xiong, R.-F. Dou, and D. G. Naugle, Liquid-assisted tip manipulation: Fabrication of twisted bilayer graphene superlattices on HOPG, Nanoscale **7**, 14865 (2015).